Inorganic Chemistry

Article

pubs.acs.org/IC

Heterometallic 3d−4f Single-Molecule Magnets: Ligand and Metal Ion Influences on the Magnetic Relaxation

Stuart K. Langley,[†] Crystal Le,[†] Liviu Ungur,[‡] Boujemaa Moubaraki,[†] Brendan F. Abrahams,[§] Liviu F. Chibotaru,*[,‡] and Keith S. Murray*[,†]

[†]School of Chemistry, Monash University, 17 Rainforest Walk, Clayton, Victoria 3800, Australia

[‡]Division of Quantum and Physical Chemistry and INPAC-Institute of Nanoscale Physics and Chemistry, Katholieke Universiteit, Leuven, Celestijnenlaan 200F, 3001 Heverlee, Belgium

[§]School of Chemistry, The University of Melbourne, Melbourne, Victoria 3010, Australia

Supporting Information

ABSTRACT: Six tetranuclear 3d−4f single-molecule magnet (SMM) complexes formed using *N*-*n*-butyldiethanolamine and *N*-methyldiethanolamine in conjunction with ortho- and para-substituted benzoic acid and hexafluoroacetoacetone ligands yield two families, both having a butterfly metallic core. The first consists of four complexes of type $\{Co^{III}_2Dy^{III}_2\}$ and $\{Co^{III}_2Co^{II}Dy^{III}\}$ using *N*-*n*-butyldiethanolamine with variation of the carboxylate ligand. The anisotropy barriers are 80 cm^{-1}, (77 and 96 cm^{-1}—two relaxation processes occur), 117 and 88 cm^{-1}, respectively, each following a relaxation mechanism from a single Dy^{III} ion. The second family consists of a $\{Co^{III}_2Dy^{III}_2\}$ and a $\{Cr^{III}_2Dy^{III}_2\}$ complex, from the ligand combination of *N*-methyldiethanolamine and hexafluoro-acetylacetone. Both show SMM behavior, the Co^{III} example displaying an anisotropy barrier of 23 cm^{-1}. The Cr^{III} complex displays a barrier of 28 cm^{-1}, with longer relaxation times and open hysteresis loops, the latter of which is not seen in the Co^{III} case. This is a consequence of strong Dy^{III}−Cr^{III} magnetic interactions, with the relaxation arising from the electronic structure of the whole complex and not from a single Dy^{III} ion. The results suggest that the presence of strong exchange interactions lead to significantly longer relaxation times than in isostructural complexes where the exchange is weak. The study also suggests that electron-withdrawing groups on both bridging (carboxylate) and terminal (β-diketonate) ligands enhance the anisotropy barrier.

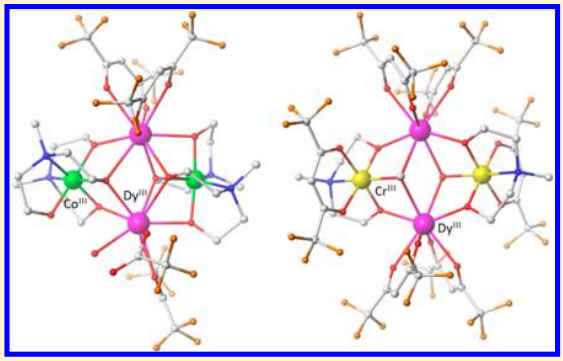

INTRODUCTION

Molecular coordination complexes that display single-molecule magnet (SMM)[1] behavior are attractive candidates for applications in high-density information storage, spin-based devices (spintronics), and quantum computation.[1,2] Many challenges need to be overcome, however, before any application can be realized, one being the very low (liquid helium) temperatures required to observe this property. Slow magnetic relaxation is observed due to an anisotropic energy barrier (U_{eff}) blocking the magnetization with a specific orientation along an easy axis. It is generally found that the larger the barrier the longer the relaxation time(s). Great interest is being shown in developing ways toward improving relaxation times from a fundamental viewpoint, by determining the factors that influence the barrier height and, hence, the relaxation time. Newly developed lanthanide coordination complexes, as well as organometallic derivatives, have proven to be particularly interesting as they have been shown to display impressive U_{eff} values[3] compared to their transition metal counterparts;[4a] though two-coordinate Fe(I) species are showing large U_{eff} values.[4b] The mechanism of slow magnetic relaxation is less understood, however, in lanthanide SMMs. Recent advances in ab initio calculations have provided a fascinating insight into the mechanism of relaxation, one involving a single-ion based mechanism,[5] a second relating to the overall magnetic exchanged within the system.[6] The single ion mechanism results from the relaxation (in most cases) via the first excited state on individual Ln^{III} ions and is dominant for systems where the magnetic exchange is weak, a common occurrence involving 4f ions.[7] When stronger magnetic exchange interactions are present, the relaxation can be outlined by connecting exchange states, resulting in a multilevel relaxation-type mechanism.[6]

Recent synthetic efforts by our group, combined with a theoretical ab initio approach, helped to develop an understanding of the mechanism of slow magnetic relaxation in complexes containing lanthanide ions. The most interesting examples explored are those of heterometallic 3d/4f "butterfly"-type coordination complexes, where the 4f ions are found in the central body positions, with the trivalent 3d ions occupying the

Received: January 29, 2015
Published: March 23, 2015

DOI: 10.1021/acs.inorgchem.5b00219
Inorg. Chem. 2015, 54, 3631−3642

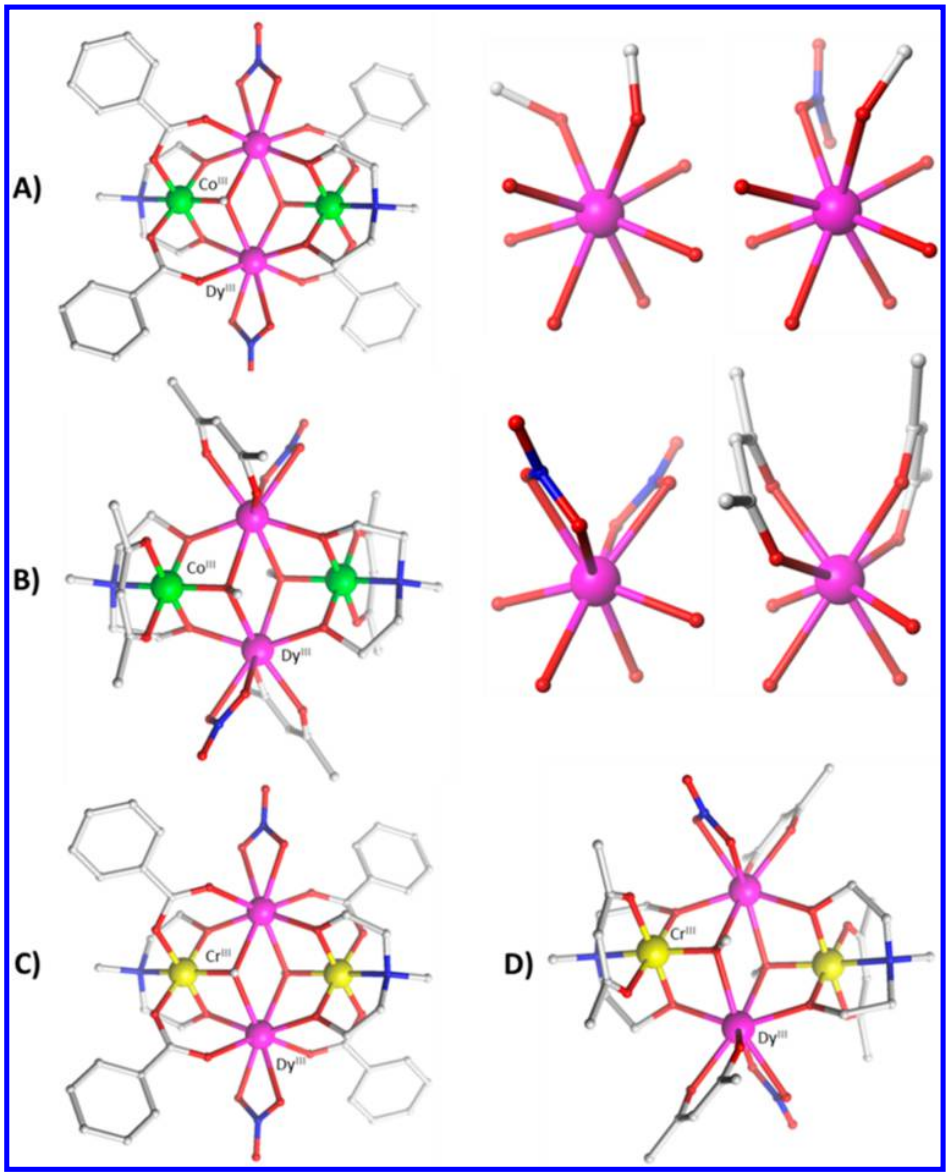

Figure 1. (A) Molecular structure of the $\{Co^{III}_2Dy^{III}_2\}$-benzoate family, with the variation in the coordination environment observed. (B) Molecular structure of the $\{Co^{III}_2Dy^{III}_2\}$-acac family, with the variation in the coordination environment observed. (C, D) Molecular structures of the Cr^{III}-substituted complexes. Variable coordination environments similar to those of (A, B) can also be observed for (C) (not shown).

outer wing positions. These can be classified into three separate complex/family types, all of which display SMM behavior. The first such family developed utilized benzoate and amine polyalcohol coligands and resulted in complexes of the type $\{Co^{III}_2Dy^{III}_2\}$-benzoate.[8] It was found that changes in the coordination sphere around the Dy^{III} ions (Figure 1A), a consequence of varying the amine−polyalcohol ligand, affected the magnitude of the anisotropy barrier. Ab initio calculations subsequently determined that the relaxation mechanism in these complexes was single ion in origin, later backed up by experimental observations, via dilution experiments.[8] This was further explored in a similar but subtly different set of $\{Co^{III}_2Dy^{III}_2\}$-acac butterfly complexes, utilizing acetylacetone (acacH) instead of benzoate, and the same amine−polyalcohol ligands (Figure 1B). In this case it was found that the terminal substituents coordinated to the Dy^{III} ions had a marked influence on the barrier height and hence on the relaxation time.[9] A third study involved the replacement of Co^{III} with Cr^{III} in both of the above-mentioned families, resulting in the analogous $\{Cr^{III}_2Dy^{III}_2\}$-benzoate and $\{Cr^{III}_2Dy^{III}_2\}$-acac complexes (Figure 1C,D). Both of these Cr^{III}-based families displayed barrier heights of similar magnitude to their Co^{III} counterparts; however, a substantial increase in relaxation times was observed, especially at very low temperatures. This was due to a change in the relaxation mechanism going from a single ion process for $\{Co^{III}_2Dy^{III}_2\}$ to a multilevel exchange mechanism for $\{Cr^{III}_2Dy^{III}_2\}$.[10] Furthermore, it was found that magnetic hysteresis could be observed with large coercive fields as a consequence of the reduced efficiency of quantum tunnelling of the magnetization (QTM) in the Cr^{III} species.[10]

A general reaction scheme highlighting the synthesis of the various butterfly complexes is given in Scheme 1. There is good chemical control in these cluster syntheses. Thus, following previous work that focused upon the replacement of the amine−

DOI: 10.1021/acs.inorgchem.5b00219
Inorg. Chem. 2015, 54, 3631−3642

Scheme 1. Synthesis of Reported $\{TM^{III}_2Ln^{III}_2\}^a$ SMMs[8−10]

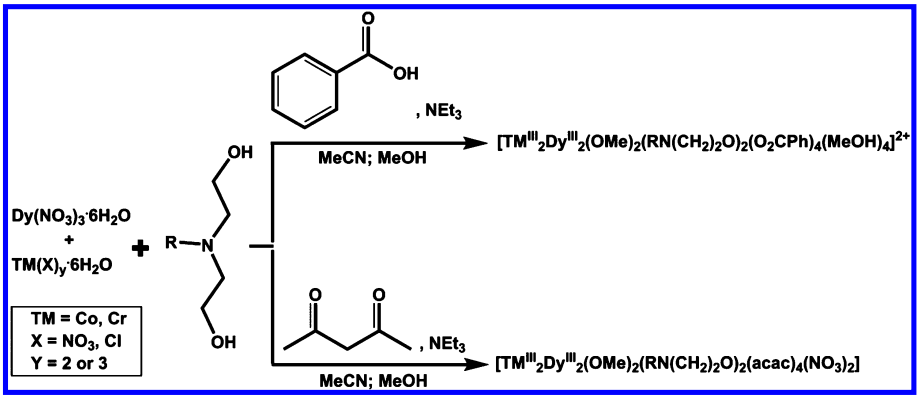

[a]Each of the resulting complexes display planar diamond/butterfly metallic core arrangements (see Figure 1). The product complexes (top) can have various combinations of MeOH and NO_3, e.g., $(MeOH)_4$ or $(MeOH)_2(NO_3)_2$; and (bottom) combinations such as $(acac)_4(NO_3)_2$ or $(acac)_2(NO_3)_4$ or $(acac)_6$.

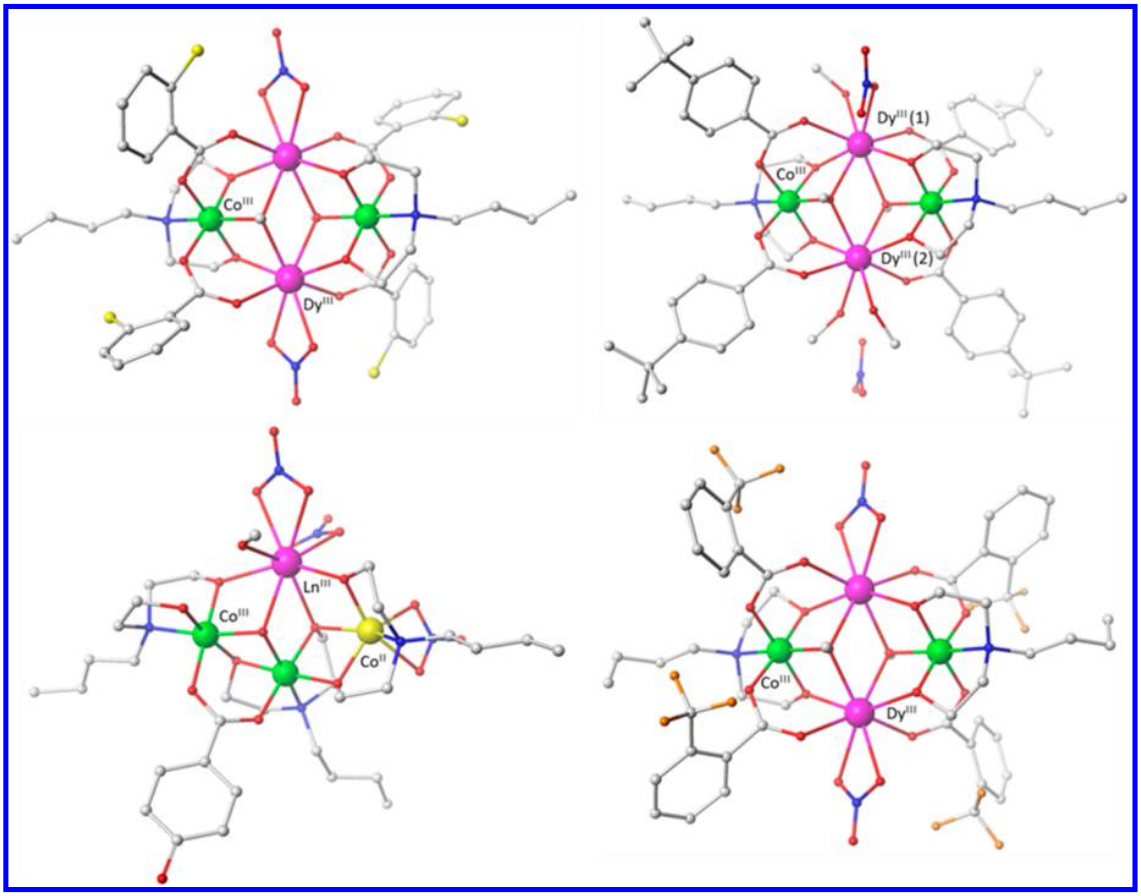

Figure 2. Molecular structure of **1** (upper left), **2** (upper right), (**3** and **3a**) (lower left), and **4** (lower right). The H atoms and solvent molecules are omitted for clarity. Color scheme; Co^{II}, yellow; Co^{III}, green; Dy^{III} (Gd^{III}), purple; O, red; N, blue; C, gray; F, orange.

polyalcohol ligand,[8b] we probed the influence that the carboxylic acid and β-diketonate ligands have on the slow relaxation of the magnetization. Herein we report the synthesis and magnetic characterization of several new tetranuclear 3d−4f butterfly SMMs, with transition metal (TM) = Co, Cr, and we make extensive comparisons of their barrier height and relaxation properties to those recently reported for related species, with ab initio calculations used to quantify the energy levels, magnetic anisotropy, and intracluster exchange coupling. We highlight the subtle but important influences brought about by electron-withdrawing substituent groups on the carboxylic acid and β-diketonate coligands, as well as the importance of exchange coupling, particularly in the $\{Cr_2Dy_2\}$ examples, that leads, experimentally, to magnetic hysteresis and, mechanistically, to a multi exchange-level relaxation mechanism, vide supra.

DOI: 10.1021/acs.inorgchem.5b00219
Inorg. Chem. 2015, 54, 3631−3642

■. RESULTS AND DISCUSSION

Synthesis. Compounds **1**−**4** were synthesized following the synthetic procedure developed for several $\{Co^{III}_2Dy^{III}_2\}$-benzoate complexes.[8] Variation of the carboxylic acid in the present study resulted in four new coordination complexes being formed, each with subtly different structural features. Compounds **1**−**4** each share a common amine−polyalcohol ligand, namely, *N*-*n*-butyldiethanolamine ($bdeaH_2$), while 2-chlorobenzoic acid (**1**), 4-*tert*-butylbenzoic acid (**2**), 4-hydroxybenzoic acid (**3**), and 2-(trifluoromethyl)benzoic acid (**4**) were utilized as the carboxylic acids. Compounds **5** and **6** follow the synthetic procedures used to isolate a series of $\{TM^{III}_2Dy^{III}_2\}$-acac (TM = Co or Cr) complexes,[9a,10c] using *N*-methyldiethanolamine ($mdeaH_2$) and with hexafluoroacetylacetone (hfacacH) used in place of acacH. The solid-state structures of **1**−**6** were determined via X-ray diffraction measurements (for crystallographic data and information see Supporting Information, Table S1). Structural elucidation revealed the formation of six new heterometallic 3d/4f complexes of formulas $[Co^{III}_2Dy^{III}_2(OMe)_2(O_2CPh\text{-}2\text{-}Cl)_4(bdea)_2(NO_3)_2]$ (**1**), $[Co^{III}_2Dy^{III}_2(OMe)_2(O_2CPh\text{-}4\text{-}^tBu)_4(bdea)_2(NO_3)(MeOH)_3](NO_3)\cdot H_2O\cdot MeOH$ (**2**), $[Co^{III}_2Co^{II}Ln^{III}(OH)(O_2CPh\text{-}4\text{-}OH)(bdea)_3(NO_3)_3(MeOH)]$ (**3**, Ln = Dy and **3a**, Ln = Gd), $[Co^{III}_2Dy^{III}_2(OMe)(OH)(O_2CPh\text{-}2\text{-}Cl)_4(bdea)_2(NO_3)_2]\cdot MeOH$ (**4**), $[Co^{III}_2Dy^{III}_2(mdea)_4(hfacac)_3(O_2CCF_3)(H_2O)]\cdot MeOH$ (**5**), and $[Cr^{III}_2Dy^{III}_2(OMe)_2(mdea)_2(hfacac)_6]$ (**6**).

Crystal Structure Descriptions. We divided the complexes into two groups, where substitution of the carboxylate ligand corresponds to complexes **1**−**4**, and use of the hfacacH ligand corresponds to **5** and **6**.

Descriptions of 1−4. Compound **1** (Figure 2, upper left) crystallizes in the triclinic space group $P\bar{1}$ and is found to be a heterometallic tetranuclear complex with two Co^{III} and two Dy^{III} ions. The asymmetric unit contains half of the cluster that lies upon an inversion center, with one unique Dy^{III} and Co^{III} ion. No solvent molecules are found in the lattice. The metallic core displays a butterfly or planar diamond type arrangement, with the Dy^{III} ions lying in the central body positions and the Co^{III} sites at the outer wing sites. The Co^{III} and Dy^{III} sites are bridged via two μ_3 methoxide ligands, each coordinating two Dy^{III} ions to a single Co^{III} ion. The metal ions are further stabilized around the periphery by two $[bdeaH]^{2-}$ ligands that coordinate via the N atom to the Co^{III} ions and then bridge the Co^{III} to the Dy^{III} ions via two μ_2 O atoms. Four 2-chlorobenzoate ligands each bridge a Co^{III} and a Dy^{III} ion, and a chelating nitrate ion coordinates to the two remaining coordination sites around each Dy^{III} ion. The Dy^{III} sites are eight coordinate, with distorted square antiprismatic geometries. The Co^{III} ions are six-coordinate with octahedral geometries.

Compound **2** (Figure 2, upper right) crystallizes in the monoclinic space group $P2_1/n$, with the entire cluster found in the asymmetric unit. The metal topology is identical to that of **1**, and the ligands are found to bridge in the same manner. The distinguishing feature of **2** lies in the coordination sphere around the Dy^{III} ions. Two unique coordination environments are found for each ion, the difference between the two lying in the terminally coordinated ligands. The first, Dy(1), contains a nitrate and methanol ligand, while the second, Dy(2), contains two methanol ligands. The complex, overall, is cationic, with a single nitrate anion balancing the charge. Both Dy^{III} sites are eight-coordinate with distorted square antiprismatic geometries. The Co^{III} ions are six-coordinate with octahedral geometries.

Compound **3** (Figure 2, lower left) crystallizes in the monoclinic space group $P2_1/c$ with the entire cluster found in the asymmetric unit. The complex again displays a butterfly metallic core but interestingly reveals a distinct arrangement of metal ions, with a significantly different bridging ligand backbone. From the X-ray data it is found that two Co^{III} ions, a Co^{II}, and a Dy^{III} ion are present. The body of the butterfly consists of a Co^{III} and a Dy^{III} ion, while the outer wing sites consist of a Co^{III} and a Co^{II} ion. A single μ_3 hydroxide ligand is found bridging the body Co^{III} and Dy^{III} ions to the outer Co^{III} ion, while three $[bdea]^{2-}$ ligands bridge to all the metal ions, displaying three modes of bonding, namely, μ_4:η^3:η^2:η^1, μ_3:η^2:η^2:η^1, and μ_2:η^2:η^1:η^1. The single carboxylate ligand bridges the two Co^{III} ions with the common μ_2 *syn*, *syn*, mode. Three chelating nitrate ligands are also found, one coordinating to the Co^{II} and two to the same Dy^{III} ion. A terminal MeOH ligand also bonds to the Dy^{III} ion. The Co^{II} and the two Co^{III} ions are six-coordinate, each with $\{CoO_5N\}$ coordination environments, with distorted octahedral geometries. The Dy^{III} ion is nine-coordinate with a capped square antiprismatic geometry. Given the similar nature of the para-substituted benzoate ligand used to that in **2**, the reasons for the structural differences are unknown.

Compound **4** (Figure 2, lower right) crystallizes in the triclinic space group $P\bar{1}$. The asymmetric unit contains half of the cluster, which lies upon an inversion center, with one unique Dy^{III} and Co^{III} ion. The metal topology is identical to that of **1** and **2**, with the same bridging ligand environment. A single chelating nitrate is coordinated to each Dy^{III} ion in a similar manner to that of complex **1**. Both Dy^{III} sites are eight-coordinate with distorted square antiprismatic geometries. The Co^{III} ions are six-coordinate with an octahedral geometry.

Analysis of the four compounds revealed that variation of the benzoic acid ligand resulted in modification of the coordination environment (**1**, **2**, and **4**) as well as in the arrangement of ions in the cluster topology, highlighted by **3**. Upon comparison of **1**, **2**, and **4** to the previously reported $\{Co^{III}_2Dy^{III}_2\}$-benzoate-bdea complex(es),[8b] we find we can change the coordination environment around the Dy^{III} centers via simple variation of the carboxylic acid. The previous benzoate example revealed two related but unique molecules of formulas $[Dy^{III}_2Co^{III}_2(OMe)_2(bdea)_2(O_2CPh)_4(MeOH)_4](NO_3)_2$ and $[Dy^{III}_2Co^{III}_2(OMe)_2(bdea)_2(O_2CPh)_4(MeOH)_2(NO_3)_2]$ within the same crystal (Supporting Information, Figure S1).[8b] In the present study the use of ortho- and para-substituted benzoate ligands shows, first, that we can isolate one unique molecule in the asymmetric unit, either an asymmetric complex, with two unique Dy^{III} coordination environments, or a centrosymmetric compound favored by the ortho-substituted ligands. Second, the substituted position of the benzoate ring influences the composition of the complex, with ortho-substituted benzoates preferring a chelating nitrate ligand for the completion of the coordination environment of each Dy^{III} ion. This is likely a consequence of the steric effects of the ligand.

Descriptions of 5 and 6. Complex **5** (Figure 3, left) crystallizes in the triclinic space group $P\bar{1}$, with the entire cluster found in the asymmetric unit. As with **1**−**4**, compound **5** is a heterometallic tetranuclear complex, and in this case consists of two Co^{III} and two Dy^{III} ions. The four $[mdea]^{2-}$ ligands display three modes of bonding. Two display the μ_3:η^3:η^2:η^1 mode, while the remaining two display μ_3:η^2:η^2:η^1 and μ_3:η^3:η^1:η^1 modes. Each of these ligands coordinate via the N atom to the Co^{III} ions, with the O atoms bridging the Co^{III} and Dy^{III} ions, while for one ligand a single O atom chelates, lying terminal. Three $[hfacac]^-$

DOI: 10.1021/acs.inorgchem.5b00219
Inorg. Chem. 2015, 54, 3631−3642

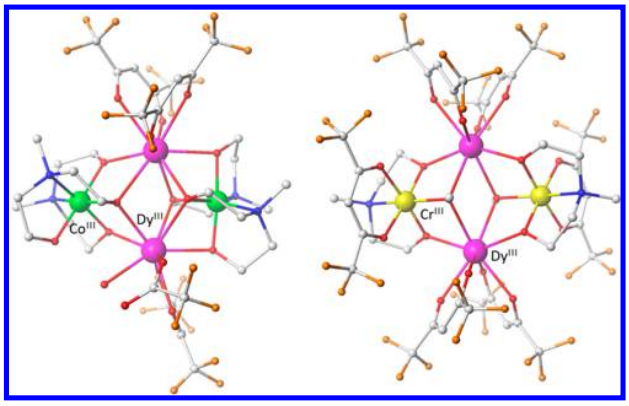

Figure 3. Molecular structure of **5** (left) and **6** (right). The H atoms, disordered, and solvent molecules are omitted for clarity. Color scheme; Cr^{III}, yellow; Co^{III}, green; Dy^{III}, purple; O, red; N, blue; C, gray; F, orange.

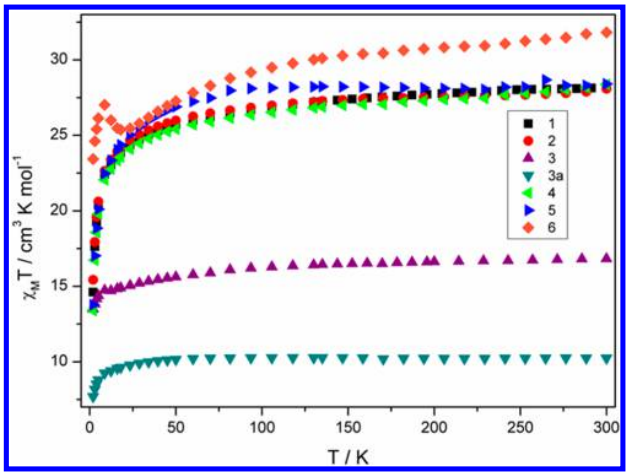

Figure 4. Plots of $\chi_M T$ vs T for **1**−**6** measured in a dc field of 0.1 T.

ligands, a trifluoroacetate ($[tfa]^-$), and a water molecule are also present, chelating and terminally bonding to the Dy^{III} sites. The presence of the $[tfa]^-$ is likely a result of hydrolysis of the hfacacH ligand. As a result of the $[tfa]^-$ ligand two unique Dy^{III} environments are found, both of which are nine-coordinate, with distorted capped square antiprismatic geometries. The Co^{III} ions are six-coordinate with octahedral geometries.

Complex **6** (Figure 3, right) crystallizes in the orthorhombic space group *Pbca*. The asymmetric unit contains half of the cluster, which lies upon an inversion center, with one unique Dy^{III} and Cr^{III} ion. The metallic core arrangement again reveals a butterfly or diamond motif, with the two Dy^{III} ions occupying the "body" positions and the Cr^{III} ions the outer "wing-tip" sites. These ions are bridged via two μ_3 methoxide ligands, each coordinating two Dy^{III} ions to a single Cr^{III} ion. The two $[mdea]^{2-}$ ligands coordinate via the N atom to the Cr^{III} ions and bridge the Cr^{III} to the Dy^{III} ions via two μ_2 O atoms. The coordination sphere of each Cr^{III} ion is completed by one chelating $[hfacac]^-$ ligand, while two chelating $[hfacac]^-$ ligands complete the coordination environment of the Dy^{III} ions. This results in six-coordinate Cr^{III} ions with octahedral geometries. The Dy^{III} ions are all eight-coordinate with distorted square antiprismatic geometries.

Several heterometallic 3d/4f complexes were earlier reported by us using amine−polyalcohol ligands and with $[acac]^-$ as a coligand (Figure 1B,D).[9,10c] Upon replacement of $[acac]^-$ with the $[hfacac]^-$ ligand the molecular structures of **5** and **6** reveal subtle differences to their $[acac]^-$ counterparts. Compound **5** displays a significantly different bridging arrangement of ligands, and hence the Dy^{III} coordination environment (eight to nine) is different from previous reports.[9] Compound **6**, while maintaining the same bridging backbone as that of previous examples, reveals two chelating $[hfacac]^-$ ligands, different than the one $[acac]^-$ and one nitrate coordinated to the Dy^{III} ion that is commonly observed.[10c]

Magnetic Measurements. The static magnetic susceptibilities of polycrystalline samples of **1**−**6** and the $\{Co^{II}Co^{III}_2Gd^{III}\}$ analogue of **3** (**3a**) were measured in the 2−300 K temperature range under applied magnetic fields of 0.1−5 T. The $\chi_M T$ versus T plots (0.1 T) of **1**−**6** are shown in Figure 4, while magnetization versus field (0.01−5 T, 2−20 K) plots are given in Supporting Information, Figures S2−S7. The results are summarized in Table 1. The sum of the Curie constants of the individual ions and the room temperature $\chi_M T$ values are in good agreement. For **1**−**5**, the $\chi_M T$ product decreases steadily with decreasing temperature due to the spin−orbit effects of the lanthanide ions (and Co^{II} ions for **3** and **3a**). Weak antiferromagnetic exchange and/or dipolar interactions are also likely to contribute to this behavior, as found in analogous complexes.[8] In the case of **6**, however, a decrease in $\chi_M T$ is followed by an increase below 20 K, suggestive of a ferrimagnetic ground state and, due to the similarity in behavior to that of analogous $\{Cr^{III}_2Dy^{III}_2\}$ complexes, the likelihood of strong intracluster magnetic exchange.[10c] The magnetization isotherm plots reveal a steady increase upon increasing field without reaching saturation at 5 T. This is common for such complexes and indicates anisotropy is present within these compounds.

To probe the slow relaxation of the magnetization and quantum tunnelling effects within these molecules variable-temperature and variable-frequency alternating current (ac) magnetic measurements were performed, utilizing a 3.5 Oe oscillating field and a zero-applied direct current (dc) magnetic field. Both the in-phase (χ_M') and out-of-phase (χ_M'') susceptibilities display a frequency and temperature dependence for **1**, **2**, **4**, **5**, and **6**, signaling that blocking of the magnetization due to an anisotropy barrier (Supporting Information, Figures S8−S13 and Figures 5 and 7). No maxima in $\chi_M''(\nu)$ were observed for **3** (Supporting Information, Figure S14); however, clear signals can be seen under the application of a bias dc field, the optimum field being found at H_{dc} = 1500 Oe (Supporting Information, Figure S15). No slow relaxation is found for complex **3a**. From these data, the relaxation times ($\tau = (2\pi\nu)^{-1}$ at $\nu = \chi_M''_{max}$) at a given temperature are plotted as $\ln(\tau)$ versus $1/T$ (Supporting Information, Figures S16 and S17). It was found that the relaxation follows a thermally activated mechanism above 11 K, (14 and 9 K), 25 K, 12.5 K, 6 K, and 1.8 K for **1**−**6**, respectively, with plots of $\ln(\tau)$ versus $1/T$ being linear. These data were fitted to the Arrhenius law [$\tau = \tau_o \times \exp(U_{eff}/k_BT)$], which allowed for the evaluation of the anisotropy barrier (U_{eff}) and pre-exponential factor (τ_o). As the temperature was reduced, complexes **1**−**5** displayed a crossover toward a temperature-independent regime, as evidenced, first at intermediate temperatures by a curvature in the $\ln(\tau)$ versus $1/T$ plot, where thermal and quantum tunnelling mechanisms are active concurrently. The relaxation then became independent of temperature, indicative of a purely quantum tunnelling relaxation mechanism when the temperature approaches 1.8 K (see Figures S16 and S17 in Supporting Information).

DOI: 10.1021/acs.inorgchem.5b00219
Inorg. Chem. 2015, 54, 3631−3642

Table 1. Magnetic Data Recorded for Compounds 1−6

	dc susceptibility data				ac susceptibility data		
compound	Curie constant expected for the complex (cm^3 K mol^{-1})	observed $\chi_M T$ (cm^3 K mol^{-1}) at 300 K	observed $\chi_M T$ (cm^3 K mol^{-1}) at 2 K	observed M ($N\mu_B$) at 2 K and 5 T	U_{eff} (applied field), cm^{-1}	τ_o, s	τ_{QTM}, s
1	28.3	28.2	14.6	10.4	80.4 (0 Oe)	1.8×10^{-8}	0.9
2	28.3	28.1	15.4	10.3	76.9 and 95.6 (0 Oe)	3.8×10^{-9} s and 5.6×10^{-8}	0.5 and n/a[a]
3	16.0 (g = 2 for Co^{II})	16.8	13.5	7.5	117.4 (1500 Oe)	3.4×10^{-7}	0.3
3a	9.8 (g = 2 for Co^{II})	10.2	7.7	9.2	n/a	n/a	n/a
4	28.3	28.3	13.4	10.4	88.1 (0 Oe)	1.4×10^{-8}	∼1.5
5	28.3	28.4	13.8	10.8	22.6 (0 Oe)	1.4×10^{-6}	0.004
6	32.1	31.8	23.4	9.6	28.6 (0 Oe)	1.6×10^{-7}	n/a

[a]n/a indicates not applicable.

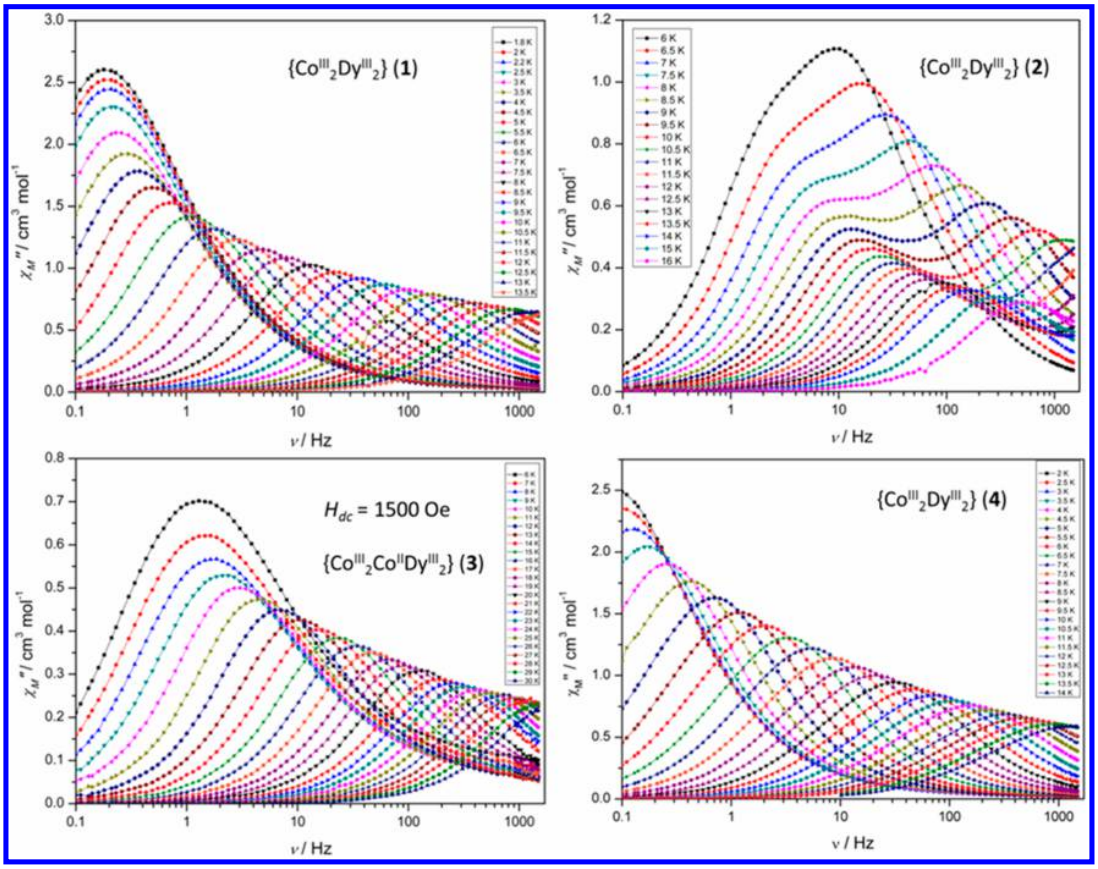

Figure 5. Comparison of the frequency dependence of the out-of-phase (χ_M'') susceptibilities of **1** (upper left), **2** (upper right), **3** (lower left), and **4** (lower right).

Fast QTM is a common observation in Ln^{III} SMMs, and a pure quantum regime occurs when the tunnelling rate becomes faster than the thermally activated process. The data points that are fitted to the regression line in the higher-temperature region are taken to the largest *R*-squared value. At the point where this value drops off due to the curvature of the plot, these data are omitted from the Arrhenius analysis. No crossover to a pure quantum regime is observed for compound **6**. The parameters extracted from the ac relaxation data are tabulated in Table 1.

Evaluation of the Dynamic Magnetic Data for 1−4. We had shown previously that the magnetic relaxation in a family of {$Co^{III}_2Dy^{III}_2$} complexes (low-spin Co^{III} is diamagnetic) is due to the large Dy^{III} single ion anisotropy, in the appropriate ligand field environment, and not of the coupled system, a consequence of the weak Dy···Dy magnetic exchange present.[8] Through a combination of experiment and theory, a relationship was found revealing that the barrier height is correlated to the ground-to-first excited-state energy gap of the lowest Dy^{III} Kramers doublets.[8b] This ground state-to-excited state gap could then be modulated by the ligands that coordinate to the Dy^{III} ions. A simple perusal of the present structures determined that **1** and **4** display the same coordination environment at the Dy^{III} sites, but both differ from that of **2**. As stated, this simple chemical difference can lead to vastly different SMM behavior, one of our goals at the outset. It is also noted that **1** and **4** contain different

DOI: 10.1021/acs.inorgchem.5b00219
Inorg. Chem. 2015, 54, 3631−3642

ortho-substituted groups on the benzoate ligands, which may influence the electronic properties of the Dy^{III} ion.[11]

Compounds **1**–**4** each display large anisotropy barriers with values of 81 cm^{-1}, (77 and 96 cm^{-1}), 117, and 88 cm^{-1}. For compound **2**, two maxima are observed in the χ_M'' versus υ isotherms, indicative of two distinct relaxation processes. The lower-frequency maximum at each particular temperature is a result of a longer relaxation time and thus is denoted as the slow process. The higher-frequency maximum at each particular temperature is a result of a shorter relaxation time and is denoted as the fast process. The lowest-temperature χ_M'' maxima points (<8 K) for the fast process are obscured, and thus no low-temperature relaxation times could be extracted. The two relaxation mechanisms of differing time scales can be rationalized by the two distinct coordination environments found for each Dy^{III} ion and the corresponding differences in the low lying electronic structure for each ion (see ab initio calculations vide infra). Compounds **1** and **4** display distinct anisotropy barrier heights, which may be rationalized by the Cl versus CF_3 substituents coordinated to the ortho-position of the benzoate ligand. This effect has recently been highlighted by Murugesu and co-workers, particularly highlighting the effect of electron-withdrawing groups directly coordinated to the Ln^{III} ion.[12]

Compound **3** displays significantly different behavior from that of **1**, **2**, and **4**, with no slow relaxation observed above 1.8 K at H_{dc} = 0 Oe, and is likely a consequence of the new coordination environment/geometry about the Dy^{III} site. The coordination changes from an eight- to a nine-coordinate capped square antiprismatic geometry, and with a significantly different ligand environment. It is found that QTM is efficient and that the application of a static dc field "turns on" the magnetic relaxation. With the inclusion of the anisotropic Co^{II} ion the use of the Co^{II}–Gd^{III} complex **3a** reveals that the origin of the slow relaxation stems from the Dy^{III} ion, as no SMM behavior is observed for the Gd^{III} analogue **3a**. While the very large relaxation barrier (118 cm^{-1}) is only observed under the application of the magnetic field, recent studies have shown that the transformation of the coordination environment via loss of terminal ligands will alter the ligand field, and hence the magnetic anisotropy, tunnelling frequency, and energy barrier.[13] This can conceivably be achieved for **3** via loss of the terminal MeOH ligand and may result in a reduction of the QTM, thus turning on the zero field relaxation.

Cole–Cole plots confirm that a single relaxation process is observed for **1**, **3**, and **4**, while two clear processes are found for **2** (Supporting Information, Figures S18–S21).

Compounds **1**, **2**, and **4** display slow relaxation of the magnetization in the absence of a static dc field, whereas compound **3** displays no such behavior. Upon application of a static dc field slow relaxation of the magnetization becomes clear. This suggests that QTM is highly efficient for **3** at zero-field (>0.1 ms). Even under the presence of a static dc field the relaxation again crosses over from a thermally activated to a quantum tunnelling relaxation process as the temperature is reduced, with a tunnelling time of 0.3 s, indicating the tunnelling mechanism is still very efficient in this sample. It is also observed that **1**, **2**, and **4** display a crossover from a thermally activated to a quantum tunnelling relaxation mechanism as the temperature is reduced. Tunnelling frequencies of 0.18, 0.30, and 0.10 Hz are found corresponding to relaxation times of 0.9, 0.5, and ∼1.5 s. The tunnelling times for these four complexes, while relatively slow for Ln-based systems, are still extremely fast when considering long relaxation times required for the storage of digital information. A point of interest to note is that in all cases the paramagnetic ions are surrounded by two diamagnetic Co^{III} ions. A recent report suggests that the presence of diamagnetic ions may influence the height of the relaxation barrier favorably.[14]

Ab initio calculations were performed for complex **2** to probe the origin of the multiple relaxation processes. The computational details are given in the Supporting Information, Table S2. The calculated electronic and magnetic properties of the two individual Dy^{III} free-ions for **2** show that the local *g*-tensors in the ground Kramers doublet are all strongly axial with a large g_z value indicating a large magnetic moment, approaching that expected for a pure $m_J = {}^{15}/_2$ state of $g_z = 20$, explaining the presence of slow magnetic relaxation. The energy spectrum of the ground $^6H_{15/2}$ multiplet and the associated Kramers doublets and *g* tensors are shown in Table 2 (also see Supporting Information, Tables S3 and S4).

Table 2. Energies of the Lowest Kramers Doublets (KD; cm^{-1}), with the *g* Tensors of the Ground Kramers Doublet for 2

	Dy(1) (basis 2)	Dy(2) (basis 2)
KD 1	0.000	0.000
KD 2	133.214	94.547
KD 3	269.182	202.895
KD 4	352.538	275.976
KD 5	406.330	318.999
KD 6	452.814	365.787
KD 7	509.949	434.321
KD 8	778.730	746.382
g tensors of KD 1	g_x 0.005 744	g_x 0.019 676
	g_y 0.006 981	g_y 0.026 176
	g_z 19.836 157	g_z 19.754 644

From the calculations it is clear that the ground to first excited state energy gap is significantly different for Dy(1) and Dy(2), and as these systems relax via phonon absorption/emission to a single excited state on individual ions, then the relaxation times are expected to be different for each ion.[8a] Thus, one can comment that the slow process stems from Dy(1) (ground → excited state; 133 cm^{-1}) and that the fast process originates from Dy(2) (ground → excited state; 94 cm^{-1}), the combined theoretical and experimental investigation nicely delineating the observed behavior. Note, however, that the calculated barriers (ground to first excited state) are slightly larger than the experimentally determined parameters; 133 and 94 cm^{-1} (calculated) versus 96 and 77 cm^{-1} (found). This overestimation has been observed on many occasions,[8b] with the experimentally determined barrier likely to be influenced by QTM, which we showed to be clearly prominent in the sample. Therefore, taking into account thermal and direct relaxation processes, the experimental barrier often does not reach that of a pure Orbach process, via the first excited state.

The orientation of the anisotropy axes for the ground Kramers doublet for each Dy^{III} ion is shown in Figure 6. The orientations of the axes are not coparallel with a deviation of 15.7° found between Dy1 and Dy2 (basis 2). (See Supporting Information, Figure S5 for the full table, with differing degrees of computational approximation.)

The ab initio wave functions and energies for all Dy^{III} sites are employed in the computation of the intramolecular magnetic interactions. The exchange interaction is treated within the Lines

DOI: 10.1021/acs.inorgchem.5b00219
Inorg. Chem. 2015, 54, 3631–3642

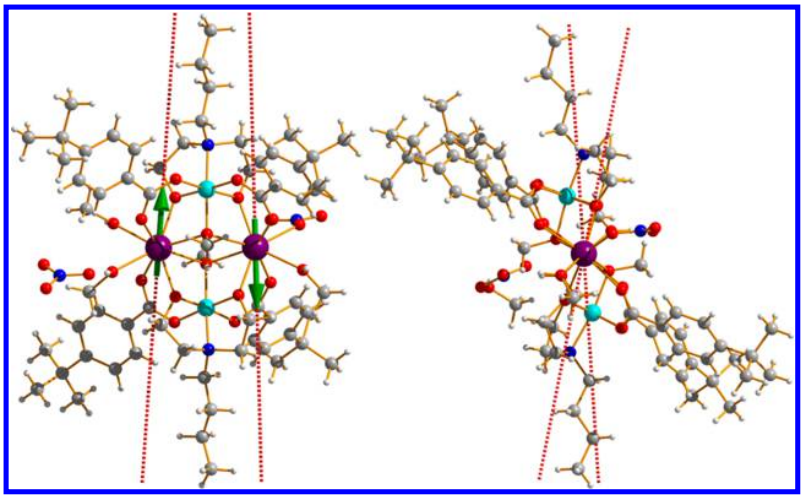

Figure 6. Orientation of the main anisotropy axes in the ground Kramers doublet of **2**. Green arrows show the antiferromagnetic coupling of the local magnetic moments of the Dy^{III} ions in the ground state.

model,[15] which describes the exchange coupling between the spin moments of magnetic sites in the absence of spin−orbit coupling by one parameter. In the case of spin−orbit coupling, the projection of the Lines model accounts for anisotropic exchange interaction between metal sites. Equation eq 1 gives the Ising exchange Hamiltonian, where the anisotropic dipolar and exchange interactions are treated within the Lines model.[15]

$$H = -(J_{dip} + J_{exch})\hat{\tilde{s}}_{1,z}\hat{\tilde{s}}_{2,z} \quad \text{(eq 1)}$$

where $\tilde{s}_{i,z} = 1/2$ is the projection of the pseudospin corresponding to the lowest Kramers doublet of each ion onto the main anisotropy axis z. The dipolar contribution is considered exactly, while the exchange part is determined from a fit to the magnetic data. All calculations were performed using the POLY_ANISO routine.[16] The calculations reproduce the susceptibility and magnetization measurements well, with fits of the magnetic data shown in Supporting Information, Figure S22. The exchange parameters obtained are summarized in Table 3.

Table 3. Exchange Interactions between Dy^{III} Ions in the Unsymmetrical Complex 2

	Ising parameters (cm^{-1})		
model	J_{dip} [a]	J_{exch}	$J_{total} = J_{dip}$ [a] $+ J_{exch}$
basis 1	−2.538 20	−0.172 96	−2.711 16
basis 2	−2.505 61	−0.226 67	−2.732 28

[a]Contribution coming only from the Ising terms $\approx \hat{\tilde{s}}_{1,z}\,\hat{\tilde{s}}_{2,z}$ to the dipolar coupling. In the calculation of the exchange spectrum (see Supporting Information, Table S7) the dipolar interaction included all terms.

The results reveal a weak antiferromagnetic interaction between the Dy^{III} ions as expected, dominated by the dipolar contribution. A noncompensation of the spins due to the noncoparallel axes allows for a nonzero magnetic ground state (g_z = 5.4), with the next higher exchange doublet state lying 1.3 cm^{-1} above the ground (g_z = 39.2). Supporting Information, Table S7 shows the low-lying exchange spectrum of the complex. This behavior differs from that in previous $\{Co_2^{III}Dy_2^{III}\}$ complexes, where a diamagnetic exchange ground state is found, with a low-lying excited magnetic state ∼1.4 cm^{-1} above the ground ($g_z \approx$ 39.3).[8]

Evaluation of the Dynamic Data for Complexes 5 and 6. Both **5** and **6** display SMM behavior with anisotropy barriers of 22 and 29 cm^{-1}, respectively. While the magnitude of the thermally activated barrier heights are similar, they display notably different relaxation profiles. Complex **6** reveals temperature-dependent relaxation over the entire frequency range (Figure 7), indicating that the complex does not cross over to a pure quantum regime on the time scale of the experiment. This results in significantly longer relaxation times below 4 K. A single relaxation process is observed from the Cole−Cole plot (Supporting Information, Figure S23). As mentioned above, and evidenced from previously studied $\{Cr_2^{III}Dy_2^{III}\}$ complexes (Figure 1C,D), one way of reducing QTM is the incorporation of strong magnetic exchange interactions. This allows for the slow magnetic relaxation to stem from the exchange coupled system and not from a single Dy^{III} ion, which, on the basis of previous studies, is also the case here.[10] It was recently shown that stronger exchange interactions translate to larger U_{eff} values offering a key pathway toward improving relaxation times.[10c]

Contrary to what is found for **6**, we again observe fast QTM (0.004 ms) in the weakly exchanged complex **5**. A second observation from the ac data for **5** is that a second relaxation process is found at higher frequencies, confirmed in the Cole−Cole plot (Supporting Information, Figure S24). It was noted in the structural description that two distinct Dy^{III} sites are present and that as the relaxation stems from a single Dy^{III} ion then multiple relaxation mechanisms are conceivable (see ab initio analysis of **2**).

Magnetic Hysteresis Measurements. In view of all present compounds displaying slow magnetic relaxation on a short time scale (ac data), with large thermal anisotropy barriers, we also probed to see if slow magnetic relaxation is observed on a longer time scale. No hysteresis was found for polycrystalline samples of compounds **1**−**5**, above 1.8 K, using a conventional superconducting quantum interference device (SQUID) magnetometer and an average sweep rate of 0.004 T/s. Under similar conditions, however, we were able to observe $M(H)$ hysteresis loops at temperatures as high as 2.2 K for the Cr^{III} complex **6** (Figure 8). The coercive field is found to be ∼2500 Oe at 1.8 K, which decreases with increasing temperature, typical of an SMM.

DOI: 10.1021/acs.inorgchem.5b00219
Inorg. Chem. 2015, 54, 3631−3642

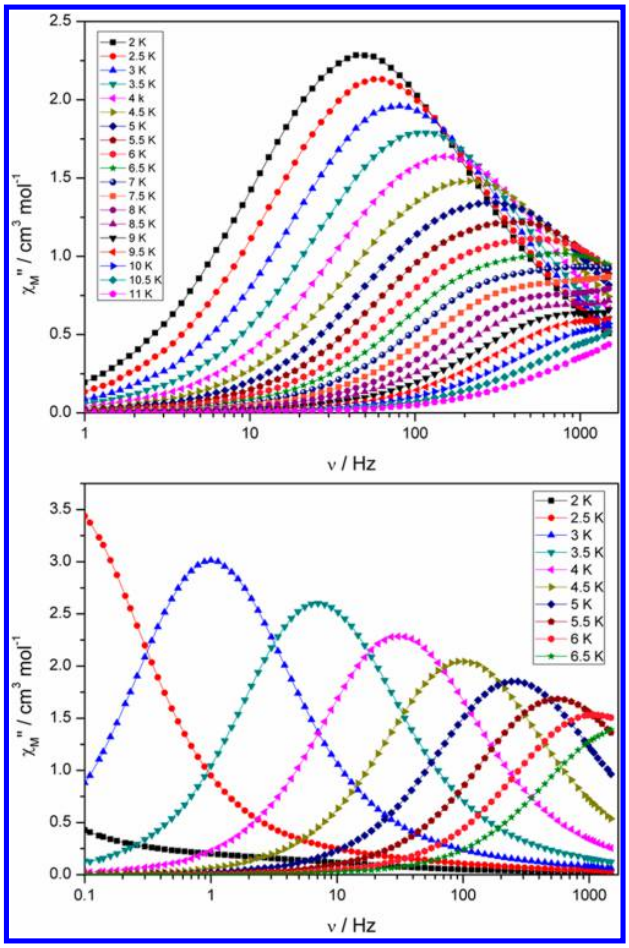

Figure 7. Frequency dependence of the out-of-phase (χ_M'') susceptibilities of **5** (upper) and **6** (lower).

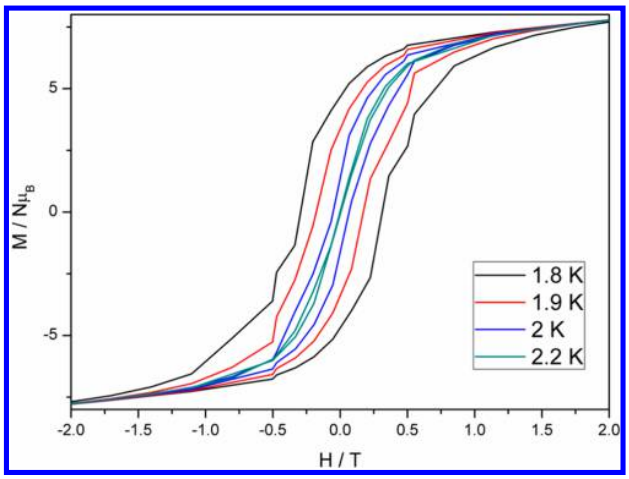

Figure 8. Plot of magnetization (M) vs field (H) for **6**, sweeping the field with an average sweep rate of 0.004 T/s, at the temperatures indicated.

These results highlight that the magnitude of the anisotropy barrier in Ln^{III}-containing systems must be taken cautiously and do not necessary translate to longer relaxation times and high hysteretic blocking temperatures (T_B). Obviously, the QTM times in these systems is a key parameter that needs to be effectively slowed or suppressed.

A large output of $\{TM_2^{III}Dy_2^{III}\}$ butterfly SMMs has now been reported in the literature, where the Dy^{III} ions occupy the body positions. To put the present results into context, a comparison of the relevant relaxation parameters for these complexes is given in Table 4. Clearly, the anisotropy barrier varies greatly for the $\{Co_2^{III}Dy_2^{III}\}$ complexes, specifically, 19 and −117 cm^{-1}. This is simply a consequence of the single ion anisotropy and the tunability that presents itself via chemical manipulation of the coordination environment around the Dy^{III} ion. It is found for **1**, where 2-chlorobenzoate is present and when the terminal coordinating group on the Dy^{III} ion is a chelating nitrate, the barrier is larger when compared to the benzoate example (55 vs 80 cm^{-1}). A further improvement is then observed for **4** (88 cm^{-1}), also containing a chelating nitrate and 2-trifluoromethylbenzoate as the carboxylate. This adds support to conclusions reported by Murugesu and Powell in which substituent groups on peripheral ligands clearly affect the direction of the anisotropy axis.[11,12] It has been noted, particularly, that electron-withdrawing groups have a positive effect on the barrier height,[12] a trend that is found in the present study; U_{eff} for 2-trifluoromethylbenzoate >2-chlorobenzoate > benzoate. No direct comparison can be made to complexes **3** and **5** due to the uniqueness of these structures.

The U_{eff} value for the two groups of $\{Cr_2^{III}Dy_2^{III}\}$ complexes remain relatively constant due to the greater difficultly in directly affecting the magnetic exchange interaction (43−54 cm^{-1} and 24−29 cm^{-1}).[10a,c] An interesting observation is detected when comparing **6** to the analogous $[Cr_2^{III}Dy_2^{III}(OMe)_2(acac)_4(mdea)_2(NO_3)_2]$ complex (Supporting Information, Figure S25). For **6** the $[acac]^-$ and nitrate ligands were replaced by the $[hfacac]^-$ ligand, and it is found that the barrier height is greater in magnitude (29 vs 24 cm^{-1}), suggestive of stronger exchange interactions. As a consequence the blocking temperature increases from 1.8 to 2.2 K. Therefore, the addition of electron-withdrawing groups offers a potential avenue toward improving the exchange strength and hence the anisotropy barrier in exchange type relaxation processes involving anisotropic Ln^{III} ions. Further experimental evidence needs to be presented, but the present results from both single ion (Co^{III}) and exchange-coupled (Cr^{III}) systems reveal that electron-withdrawing groups decorating the peripheral ligands affect the anisotropy barrier favorably and can be used to enhance relaxation times.

■. SUMMARY AND CONCLUSIONS

This study highlights the influence of the ligand on the structure and magnetic properties of tetranuclear 3d−4f butterfly complexes. The choice of the substituted benzoate ligand allows a manner of structural control in the $\{Co_2^{III}Dy_2^{III}\}$ complexes. If ortho substituents are chosen then a chelating nitrate ligand is found in the coordination sphere of the Dy^{III} ion. If para substituents are chosen then variable Dy^{III} environments are found, and in one case a major structural rearrangement is observed. Both of these observations show that the carboxylate significantly influences the structure of these complexes. A second series of compounds is described here using fluorinated β-diketonate ligands revealing a new structural type for both a $\{Co_2^{III}Dy_2^{III}\}$ complex and a new $\{Cr_2^{III}Dy_2^{III}\}$ complex, the latter analogous to a previously reported $\{Cr_2^{III}Dy_2^{III}\}$-acac complex.[10c] Compounds **1**−**6** (with the exception of **3a**) display SMM behavior, with large anisotropy barriers. It is found that electron-withdrawing groups on the benzoate ligand enhances the anisotropy barrier in $\{Co_2^{III}Dy_2^{III}\}$ examples. It also found that

DOI: 10.1021/acs.inorgchem.5b00219
Inorg. Chem. 2015, 54, 3631−3642

Table 4. Heterometallic $\{TM_2^{III}Dy_2^{III}\}$ Butterfly SMMs, with the Dy^{III} Ions Found in the Body Position That Have Been Reported in the Literature

molecular formula[a]	U_{eff}, cm^{-1}	τ_{QTM}, s	T_B, K	ref
$[Co_2^{III}Dy_2^{III}(OMe)_2(O_2CPh)_4(teaH)_2(MeOH)_4](NO_3)_2$ and $[Co_2^{III}Dy_2^{III}(OMe)_2(O_2CPh)_4(teaH)_2(NO_3)_2(MeOH)_2]$	61	>1.5	*b*	8a, b
$[Co_2^{III}Dy_2^{III}(OMe)_2(O_2CPh)_4(dea)_2(MeOH)_4](NO_3)_2$	72	0.12	*b*	8b
$[Co_2^{III}Dy_2^{III}(OMe)_2(O_2CPh)_4(mdea)_2(NO_3)_2]$	55	0.2	*b*	8b
$[Co_2^{III}Dy_2^{III}(OMe)_2(O_2CPh)_4(bdea)_2(MeOH)_4](NO_3)_2$ and $[Co_2^{III}Dy_2^{III}(OMe)_2(O_2CPh)_4(bdea)_2(NO_3)_2(MeOH)_2]$	80	0.48	*b*	8b
$[Co_2^{III}Dy_2^{III}(OMe)_2(O_2CPh\text{-}2\text{-}Cl)_4(bdea)_2(NO_3)_2]$	80	0.9	*b*	this work
$[Co_2^{III}Dy_2^{III}(OMe)_2(O_2CPh\text{-}4\text{-}^tBu)_4(bdea)_2(NO_3)(MeOH)_3](NO_3)$	77 and 96	0.5	*b*	this work
$[Co_2^{III}Co^{II}Dy^{III}(OH)(O_2CPh\text{-}4\text{-}OH)(bdea)_3(NO_3)_3(MeOH)]$	117 (1500 Oe)	0.3 (1500 Oe)	*b*	this work
$[Co_2^{III}Dy_2^{III}(OMe)_2(O_2CPh\text{-}2\text{-}CF_3)_4(bdea)_2(NO_3)_2]$	88	~1.5	*b*	this work
$[Co_2^{III}Dy_2^{III}(OMe)_2(acac)_4(mdea)_2(NO_3)_2]$	26	0.0025	*b*	9a
$[Co_2^{III}Dy_2^{III}(OMe)_2(acac)_4(teaH)_2(NO_3)_2]$	19	0.000 58	*b*	9a
$[Co_2^{III}Dy_2^{III}(OH)_2(acac)_2(bdea)_2(NO_3)_4]$	117	>1.5 s	*b*	9b
$[Co_2^{III}Dy_2^{III}(mdea)_4(hfacac)_3(O_2CCF_3)(H_2O)]$	23	0.004	*b*	this work
$[Co_2^{III}Dy_2^{III}(OMe)_2(teaH)_2(piv)_6]$	35 and 88	*c*	*b*	17
$[Cr_2^{III}Dy_2^{III}(OMe)_2(O_2CPh)_4(mdea)_2(NO_3)_2]$	54	*c*	3.7	10a
$[Cr_2^{III}Dy_2^{III}(OMe)_2(O_2CPh)_4(dea)_2(NO_3)_2]$	43	*c*	3.5	10b
$[Cr_2^{III}Dy_2^{III}(OMe)_2(O_2CPh)_4(bdea)_2(NO_3)_2]$	43	*c*	3	10b
$[Cr_2^{III}Dy_2^{III}(OMe)_2(O_2CPh)_4(teaH)_2(NO_3)_2]$	44	*c*	3.5	10b
$[Cr_2^{III}Dy_2^{III}(OMe)_2(acac)_4(mdea)_2(NO_3)_2]$	24	*c*	1.8	10c
$[Cr_2^{III}Dy_2^{III}(OMe)_2(acac)_4(edea)_2(NO_3)_2]$	29	*c*	2.2	10c
$[Cr_2^{III}Dy_2^{III}(OMe)_2(acac)_4(bdea)_2(NO_3)_2]$	26	*c*	2.2	10c
$[Cr_2^{III}Dy_2^{III}(OMe)_2(mdea)_2(hfacac)_6]$	29	*c*	2.2	this work

[a] $edeaH_2$ = ethyldiethanolamine; $deaH_2$ = diethanolamine; $teaH_3$ = triethanolamine; pivH = pivalic acid. [b] Denotes no hysteresis is observed above 1.8 K when measured on a polycrystalline sample in a SQUID, with an average sweep rate of 0.004 T/s. [c] Denotes no pure quantum tunnelling relaxation regime is observed above 1.8 K.

QTM becomes the dominant relaxation mechanism at low temperatures. More interestingly, the $\{Cr_2^{III}Dy_2^{III}\}$ complex reveals an absence of QTM at low temperatures, and long relaxation times are thus observed. This is a consequence of strong magnetic exchange between the Cr^{III} and Dy^{III} ions, confirming the findings of our recent study.[10c] The use of electron-withdrawing groups in the Cr^{III} complex also results in longer relaxation times in comparison to an analogous compound. Two important messages can be gleaned from this work. The most salient is that the presence of stronger exchange interactions in 3d−4f complexes, $\{Cr_2Dy_2\}$ in this study, resulted in significantly longer relaxation times and the observation of open hysteresis loops, when in comparison to isostructural $\{Co_2Dy_2\}$ complexes, where the exchange is much weaker. Second it is found that the addition of electron-withdrawing groups affects the height of the relaxation barrier favorably, affecting either the single ion electronic behavior or influencing the magnitude of the exchange strength. Both of these factors should be taken into account for the design of future SMMs. Finally, we note that the present conclusions apply to Dy^{III}-containing SMMs and may well be different for other Ln^{III} species.

EXPERIMENTAL SECTION

General Information. All reactions were carried out under aerobic conditions. Chemicals and solvents were obtained from commercial sources and used without further purification. Elemental analyses (C, H, N) were carried out by Campbell Microanalytical Laboratory, University of Otago, Dunedin, New Zealand.

*Synthesis of $[Co_2^{III}Dy_2^{III}(OMe)_2(O_2CPh\text{-}2\text{-}Cl)_4(bdea)_2(NO_3)_2]$ (**1**).* $Co(NO_3)_2{\cdot}6H_2O$ (0.14 g, 0.5 mmol) and $Dy(NO_3)_3{\cdot}6H_2O$ (0.22 g, 0.50 mmol) were dissolved in MeCN (20 mL), followed by the addition of *N*-*n*-butyldiethanolamine (0.08 mL, 0.50 mmol), 2-chlorobenzoic acid (0.16 g, 1.0 mmol), and triethylamine (0.28 mL, 2.00 mmol). A green solution resulted, which was stirred for 2 h. After this time the solvent was removed yielding a green oil. This was redissolved in MeOH and layered with diethyl ether (Et_2O). Within 5−7 d green crystals of **1** had appeared, in approximate yield of 37%. Anal. Calcd (found) for **1**: $Co_2Dy_2C_{46}H_{56}O_{20}N_4Cl_4$: C, 35.20 (35.49); H, 3.60 (3.67); N, 3.57 (3.69)%.

*Synthesis of $[Co_2^{III}Dy_2^{III}(OMe)_2(O_2CPh\text{-}4\text{-}^tBu)_4(bdea)_2(NO_3)(MeOH)_3](NO_3){\cdot}H_2O{\cdot}MeOH$ (**2**).* The synthesis used for **1** was followed, but 4-*tert*-butylbenzoic acid (0.18 g, 1 mmol) was used in place of 2-chlorobenzoic acid. Green crystals of **2** appeared within 2−3 d, in approximate yield of 43%. Anal. Calcd (found) for **2**: $Co_2Dy_2C_{66}H_{110}O_{25}N_4$: C, 43.98 (44.20); H, 6.15 (6.32); N, 3.11 (3.12)%.

*Synthesis of $[Co_2^{III}Co^{II}Dy^{III}(OH)(O_2CPh\text{-}4\text{-}OH)(bdea)_3(NO_3)_3(MeOH)]$ (**3**).* The synthesis for **1** was followed, but 4-hydroxybenzoic acid (0.14 g, 1 mmol) was used in place of 2-chlorobenzoic acid. Green crystals of **3** appeared within 2−3 d from a $MeOH/CH_2Cl_2$ solution, in approximate yield of 43%. Anal. Calcd (found) for **3**: $Co_3DyC_{32}H_{61}O_{20}N_6$: C, 32.32 (32.20); H, 5.17 (5.12); N, 7.06 (7.12)%.

*Synthesis of $[Co_2^{III}Co^{II}Gd^{III}(OH)(O_2CPh\text{-}4\text{-}OH)(bdea)_3(NO_3)_3(MeOH)]$ (**3a**).* The synthesis for **3** was followed, but $Gd(NO_3)_3{\cdot}6H_2O$ (0.22 g, 0.50 mmol) was used in place of $Dy(NO_3)_3{\cdot}6H_2O$. Green crystals of **3a** appeared within 2−3 d from a $MeOH/CH_2Cl_2$ solution, in approximate yield of 53%. Anal. Calcd (found) for **3a**: $Co_3GdC_{32}H_{61}O_{20}N_6$: C, 32.46 (32.54); H, 5.19 (5.28); N, 7.10 (7.15)%.

*Synthesis of $[Co_2^{III}Dy_2^{III}(OMe)(OH)(O_2CPh\text{-}2\text{-}CF_3)_4(bdea)_2(NO_3)_2]{\cdot}MeOH$ (**4**).* The synthesis for **1** was followed, but 2-trifluoromethylbenzoic acid (0.19 g, 1 mmol) was used in place of 2-chlorobenzoic acid. Green/blue crystals of **4** appeared within 5−7 d, in approximate yield of 55%. Anal. Calcd (found) for **4**: $Co_2Dy_2C_{50}H_{58}O_{21}N_4F_{12}$: C, 34.87 (34.20); H, 3.40 (3.52); N, 3.25 (3.41)%.

*Synthesis of $[Co_2^{III}Dy_2^{III}(mdea)_4(hfacac)_3(O_2CCF_3)(H_2O)]{\cdot}MeOH$ (**5**).* $Co(NO_3)_2{\cdot}6H_2O$ (0.14 g, 0.5 mmol) and $Dy(NO_3)_3{\cdot}6H_2O$ (0.22 g, 0.5 mmol) were dissolved in MeOH (20 mL), followed by the addition of *N*-methyldiethanolamine (0.06 mL, 0.5 mmol), hexafluoroacetylacetone (0.14 mL, 0.1 mmol), and triethylamine (0.3 mL, 2.0 mmol), resulting in a purple solution. This was stirred for 2 h, and during

DOI: 10.1021/acs.inorgchem.5b00219
Inorg. Chem. 2015, 54, 3631−3642

this time a blue/green color change was observed. The solution was subsequently layered with diethyl ether (Et_2O), and within one week dark green crystals of **5** had appeared, in approximate yield of 79%. Anal. Calcd (found) for **5**: $Co_2Dy_2C_{38}H_{53}O_{18}N_4F_{21}$: C, 26.91 (26.90); H, 3.15 (3.22); N, 3.30 (3.44)%.

Synthesis of $[Cr^{III}_2Dy^{III}_2(OMe)_2(mdea)_2(hfacac)_6]$ (**6**). $CrCl_3{\cdot}6H_2O$ (0.14 g, 0.5 mmol) and $Dy(NO_3)_3{\cdot}6H_2O$ (0.22 g, 0.5 mmol) were dissolved in MeOH (20 mL), followed by the addition of *N*-methyldiethanolamine (0.06 mL, 0.5 mmol), hexafluoroacetylacetone (0.28 mL, 2 mmol), and triethylamine (0.3 mL, 2.0 mmol), resulting in a purple solution. This was stirred for 2 h under heating; over this time the solution turned blue/green. This was subsequently layered with diethyl ether (Et_2O), and within 2 d orange/red crystals of **6** had appeared, in approximate yield of 45%. Anal. Calcd (found) for **6**: $Cr_2Dy_2C_{42}H_{34}O_{18}N_2F_{36}$: C, 25.63 (25.70); H, 1.74 (1.82); N, 1.42 (1.44)%.

X-ray Crystallography. X-ray diffraction measurements for **1** were performed at 100(2) K at the Australian synchrotron MX1 beamline. The data collection and integration were performed within Blu-Ice[18] and XDS[19] software programs. Measurements for **2**, **3**, **5**, and **6** were performed using a Bruker Smart Apex X8 diffractometer at 123 K with Mo Kα radiation. The data collection and integration were performed within SMART and SAINT+ software programs and were corrected for absorption using the Bruker SADABS program. The data for **3a** and **4** were collected with an Oxford Diffraction Supernova diffractometer using Mo Kα radiation. The data collection and data reduction were performed using CrysAlisPro;[20] absorption corrections were applied using a multiscan method.[20] Compounds **1**–**6** were all solved by direct methods (SHELXS-97) and refined (SHELXL-97) by full least matrix least-squares on all F^2 data.[21] Crystallographic data and refinement parameters for **1**–**6** are summarized in Supporting Information, Table S1. Crystallographic details are available in the Supporting Information in CIF format.

Magnetic Measurements. The magnetic susceptibility measurements were performed on a Quantum Design SQUID magnetometer MPMS-XL 7 operating between 1.8 and 300 K for dc-applied fields ranging from 0 to 5 T. Microcrystalline samples were dispersed in Vaseline to avoid torquing of the crystallites. The sample mulls were contained in a calibrated gelatin capsule held at the center of a drinking straw that was fixed at the end of the sample rod. The ac susceptibility measurements were performed under an oscillating ac field of 3.5 Oe and frequencies ranging from 0.1 to 1500 Hz.

■ ASSOCIATED CONTENT

Ⓢ Supporting Information

Synopsis of this work, crystallographic data in CIF format, molecular structures of $[Co^{III}_2Dy^{III}_2(OMe)_2(O_2CPh)_4(bdea)_2(MeOH)_4](NO_3)_2$ and $[Co^{III}_2Dy^{III}_2(OMe)_2(O_2CPh)_4(bdea)_2(NO_3)_2(MeOH)_2]$, dc magnetic data for **1**–**6**, ac magnetic data for compounds **1**–**6**, Arrhenius analysis of the relaxation data for **1**–**6**, Cole–Cole plots of **1**–**4**, information regarding ab initio calculations of **2**, ab initio calculated fits of the dc magnetic data for **2**, Cole–Cole plots for **5** and **6**, molecular structure of $[Cr^{III}_2Dy^{III}_2(OMe)_2(acac)_4(mdea)_2(NO_3)_2]$. This material is available free of charge via the Internet at http://pubs.acs.org. These compounds correlate to CCDC Nos. 1025498–1025504, which can be obtained free of charge from the Cambridge Crystallographic Data Center via www.ccdc.cam.ac.uk/data_request/cif.

■ AUTHOR INFORMATION

Corresponding Authors

*E-mail: keith.murray@monash.edu. (K.S.M.)

*E-mail: liviu.chibotaru@chem.kuleuven.be (L.F.C).

Notes

The authors declare no competing financial interest.

■ ACKNOWLEDGMENTS

K.S.M thanks the Australian Research Council (ARC) and the Australia-India Strategic Research Fund (AISRF) for support of this work. L.U. and L.C. acknowledge the support of the Flemish Science Foundation (FWO) and of INPAC and Methusalem programs of the Univ. of Leuven. Part of this research was undertaken on the MX1 beamline at the Australian Synchrotron, Clayton, Victoria, Australia. Dr. W. Phonsri is thanked for assistance with graphics.

■ REFERENCES

(1) Christou, G.; Gatteschi, D.; Hendrickson, D. N.; Sessoli, R. *MRS Bull.* **2000**, *25*, 66–71.

(2) (a) Bogani, L.; Wernsdorfer, W. *Nat. Mater.* **2008**, *7*, 179–186. (b) Leuenberger, M. N.; Loss, D. *Nature* **2001**, *410*, 789–793.

(3) (a) Ganivet, C. R.; Ballesteros, B.; de la Torre, G.; Clemente-Juan, J. M.; Coronado, E.; Torres, T. *Chem.—Eur. J.* **2013**, *19*, 1457–1465. (b) Blagg, R. J.; Ungur, L.; Tuna, F.; Speak, J.; Comar, P.; Collison, D.; Wernsdorfer, W.; McInnes, E. J. L.; Chibotaru, L.; Winpenny, R. E. P. *Nat. Chem.* **2013**, *5*, 673–678. (c) Layfield, R. A. *Organometallics* **2014**, *33*, 1084–1099.

(4) (a) Milios, C. J.; Vinslava, A.; Wernsdorfer, W.; Moggach, S.; Parsons, S.; Perlepes, S. P.; Christou, E. G.; Brechin, K. *J. Am. Chem. Soc.* **2007**, *129*, 2754–2755. (b) Zadrozny, J. M.; Xiao, D. J.; Atanasov, M.; Long, G. J.; Grandjean, F.; Neese, F.; Long, J. R. *Nat. Chem.* **2013**, *5*, 577–581.

(5) For example (a) Ungur, L.; Le Roy, J. J.; Korobkov, I.; Murugesu, M.; Chibotaru, L. F. *Angew. Chem., Int. Ed.* **2014**, *53*, 4413–4417. (b) Chilton, N. F.; Langley, S. K.; Moubaraki, B.; Soncini, A.; Murray, K. S. *Chem. Sci.* **2013**, *4*, 1719–1730.

(6) Ungur, L.; Thewissen, M.; Costes, J.-P.; Wernsdorfer, W.; Chibotaru, L. F. *Inorg. Chem.* **2013**, *52*, 6328–6337.

(7) See Woodruff, D. N.; Winpenny, R. E. P.; Layfield, R. A. *Chem. Rev.* **2013**, *113*, 5110–5148 and references therein.

(8) (a) Langley, S. K.; Chilton, N. F.; Ungur, L.; Moubaraki, B.; Chibotaru, L. F.; Murray, K. S. *Inorg. Chem.* **2012**, *51*, 11873–11881. (b) Langley, S. K.; Chilton, N. F.; Ungur, L.; Moubaraki, B.; Chibotaru, L. F.; Murray, K. S. *Inorg. Chem.* **2014**, *53*, 4303–4315.

(9) (a) Langley, S. K.; Chilton, N. F.; Moubaraki, B.; Murray, K. S. *Inorg. Chem.* **2013**, *52*, 7183–7192. (b) Langley, S. K.; Chilton, N. F.; Moubaraki, B.; Murray, K. S. *Chem. Commun.* **2013**, *49*, 6965–6967.

(10) (a) Langley, S. K.; Wielechowski, D. P.; Vieru, V.; Chilton, N. F.; Moubaraki, B.; Abrahams, B. F.; Chibotaru, L. F.; Murray, K. S. *Angew. Chem., Int. Ed.* **2013**, *52*, 12014–12019. (b) Langley, S. K.; Wielechowski, D. P.; Moubaraki, B.; Abrahams, B. F.; Murray, K. S. *Aust. J. Chem.* **2014**, *67*, 1581–1587. (c) Langley, S. K.; Wielechowski, D. P.; Vieru, V.; Chilton, N. F.; Moubaraki, B.; Chibotaru, L. F.; Murray, K. S. *Chem. Sci.* **2014**, *5*, 3246–3256.

(11) Mereacre, V.; Baniodeh, A.; Anson, C. E.; Powell, A. K. *J. Am. Chem. Soc.* **2011**, *133*, 15335–15337.

(12) Habib, F.; Brunet, G.; Vieru, V.; Korobkov, I.; Chibotaru, L. F.; Murugesu, M. *J. Am. Chem. Soc.* **2013**, *135*, 13242–13245.

(13) (a) Song, Y.-M.; Luo, F.; Luo, M.-B.; Liao, Z.-W.; Sun, G.-M.; Tian, X.-Z.; Zhu, Y.; Yuan, Z.-J.; Liu, S.-J.; Xu, W.-Y.; Feng, X.-F. *Chem. Commun.* **2012**, *48*, 1006–1008. (b) Liu, J.-L.; Chen, Y.-C.; Zheng, Y.-Z.; Lin, W.-Q.; Ungur, L.; Wernsdorfer, W.; Chibotaru, L. F.; Tong, M.-L. *Chem. Sci.* **2013**, *3*, 3310–3316.

(14) Upadhyay, A.; Singh, S. K.; Das, C.; Mondol, R.; Langley, S. K.; Murray, K. S.; Rajaraman, G.; Shanmugam, M. *Chem. Commun.* **2014**, *50*, 8838–8841.

(15) Lines, M. E. *J. Chem. Phys.* **1971**, *55*, 2977–2984.

(16) Ungur, L.; Chibotaru, L. F. *POLY_ANISO program;* KU Leuven: Leuven, Belgium, 2007.

(17) Funes, A. V.; Carrella, L.; Rentschler, E.; Alborés, P. *Dalton Trans.* **2014**, *43*, 2361–2364.

(18) McPhillips, T. M.; McPhillips, S. E.; Chiu, H. J.; Cohen, A. E.; Deacon, A. M.; Ellis, P. J.; Garman, E.; Gonzalez, A.; Sauter, N. K.;

DOI: 10.1021/acs.inorgchem.5b00219
Inorg. Chem. 2015, 54, 3631–3642

Phizackerley, R. P.; Soltis, S. M.; Kuhn, P. *J. Synchrotron Radiat.* **2002**, *9*, 401−406.
(19) Kabsch, W. J. *Appl. Crystallogr.* **1993**, *26*, 795−800.
(20) Empirical absorption correction using spherical harmonics, implemented in SCALE3 ABSPACK scaling algorithm. *CrysAlisPro*, Version 1.171.33.34d (release 27−02−2009 CrysAlis171.NET); Agilent Technologies (Oxford Diffraction): Santa Clara, CA, 2009.
(21) Sheldrick, G. M. *Acta Crystallogr., Sect. A* **2008**, *A64*, 112−122.

DOI: 10.1021/acs.inorgchem.5b00219
Inorg. Chem. 2015, 54, 3631−3642